JACS
JOURNAL OF THE AMERICAN CHEMICAL SOCIETY
Communication
pubs.acs.org/JACS

Formation of Halogen Bond-Based 2D Supramolecular Assemblies by Electric Manipulation

Qing-Na Zheng,[†,‡] Xuan-He Liu,[†,‡] Ting Chen,[†] Hui-Juan Yan,[†] Timothy Cook,[§,∥] Dong Wang,*[,†] Peter J. Stang,[§] and Li-Jun Wan*[,†]

[†]Key Laboratory of Molecular Nanostructure and Nanotechnology and Beijing National Laboratory for Molecular Sciences, Institute of Chemistry, Chinese Academy of Sciences (CAS), Beijing 100190, P. R. China

[‡]Graduate University of the Chinese Academy of Sciences, Beijing 100049, China

[§]Department of Chemistry, University of Utah, 315 South 1400 East, Salt Lake City, Utah 84112, United States

[∥]Department of Chemistry, University at Buffalo, State University of New York, Buffalo, New York 14260, United States

Supporting Information

ABSTRACT: Halogen bonding has attracted much attention recently as an important driving force for supramolecular assembly and crystal engineering. Herein, we demonstrate for the first time the formation of a halogen bond-based open porous network on a graphite surface using ethynylpyridine and aryl-halide based building blocks. We found that the electrical stimuli of a scanning tunneling microscopy (STM) tip can induce the formation of a binary supramolecular structure on the basis of halogen bond formation between terminal pyridyl groups and perfluoro-iodobenzene. This electrical manipulation method can be applied to engineer a series of linear or porous structures by selecting halogen bond donor and acceptor fragments with different symmetries, as the directional interactions ultimately determine the structural outcome.

Halogen bonding (XB) is a net attractive interaction involving a halogen atom (XB donor, X) and an XB acceptor (D, such as N, O, S, P, or halogen atoms).[1] Depending on the nature of XB acceptor, XB can be categorized into two types.[2] Nucleophiles (typically N, O) can approach halogen atom approximately along the C—X bond axis, resulting in an XB angle of ca. 180°; electrophiles (typically another halogen atom) approach the halogen atom in a roughly orthogonal direction. XB is an important noncovalent interaction that contributes to the hierarchical structures of macromolecules in biological systems and the packing modes of organic crystals. It has been increasingly investigated by using crystallographic[3] and theoretical methods.[4] Recently, established XB tectons have been integrated to fabricate supramolecular materials such as organic gels, liquid crystals, and ion transporters.[5]

Noncovalent interactions play an important role in the engineering of 2D supramolecular assemblies on solid supports. Important driving forces, spanning hydrogen bonding, van der Waals interactions, and $\pi-\pi$ stacking have been used to construct a large number of highly ordered supramolecular structures. Despite the extensive exploitation of XB in the design of molecular crystals and functional supramolecular materials, our understanding of XB-driven 2D assembly is not well-established yet. XB shares many similar features with its more familiar hydrogen bonding counterpart. In addition, XB is expected to be highly directional, hydrophobic, and strength and length tunable.[1a,6] These properties made XB an excellent candidate for tailoring supramolecular structures. Thus far, the use of XB as driving force has been applied toward several monocomponent halogen—halogen bonding driven supramolecular assemblies on surfaces.[7] For example, thiophene derivatives with bromine substituents form close-packed assembly structures due to Br—Br XB.[7a,b] In most cases, the XB-based 2D supramolecular assemblies are limited to close-packed structures. Silly and co-workers succeeded in designing halogen—halogen porous nanoarchitectures by selecting two different solvents.[7d] The porous structure was stabilized by both I—I XB and dipole—dipole interactions.

From the viewpoint of surface molecular engineering, binary assembly provides a means to design a variety of topologies. By attaching donor and acceptor moieties to molecular building blocks with different symmetries, a rich library of molecular assemblies may be fabricated. Among them, the open porous network is particularly attractive as it is thermodynamically challenging and has great potential for surface host—guest chemistry. In the 1990s, Resnati et al. used perfluorohalocarbons (PFHCs) as XB donors and examined their interactions with various Lewis bases as XB acceptors. These PFHCs are now considered to be the "iconic" XB donors and can form strong XB with acceptors such as pyridyl and aldehyde functionalities. Such XB tectons have been successfully applied to fabricate supramolecular functional materials. In contrast, reports on the formation of XB-based open networks, which are believed to be energetically unfavorable compared to close-packing structures due to the close-packing principle, are rare.[10]

Herein, we demonstrated the first formation of a binary 2D XB-based network. The well-established binary XB pairs between PFHC fluorinated iodobenzene and pyrdinyl groups were chosen as tectons to fabricate a 2D open porous network on a highly oriented pyrolytic graphite (HOPG) surface. We found that the electrical stimulus of an STM tip plays an important role in inducing the formation of the XB-based structure. High-

Received: March 1, 2015
Published: May 7, 2015

DOI: 10.1021/jacs.5b02206
J. Am. Chem. Soc. 2015, 137, 6128−6131

resolution STM confirms that the binary network is sustained by XBs. Moreover, this electrical manipulation method can be expanded to a series of XB donor and acceptor systems to yield either linear or porous structures. The result presented here offers insight into the physical chemistry nature of XB and provides a new methodology to engineer XB-based supramolecular assemblies.

We chose the tritopic **3F3I** as an XB donor. The electron-withdrawing fluorine atoms in **3F3I** promote the acidity of the iodine atoms and enhance the XBs. Figure 1a shows the expected

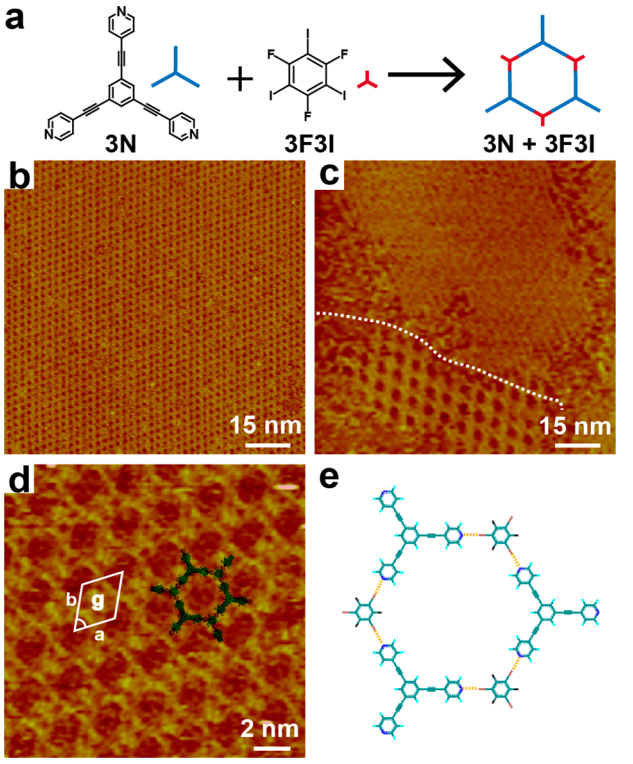

Figure 1. (a) Self-assembly of tritopic XB acceptor **3N** and XB donor **3F3I** results in the formation of a **3N**/**3F3I** honeycomb structure. (b) Large-scale STM image of the **3N**/**3F3I** honeycomb structure. Tunneling conditions: V_{bias} = 800 mV, I_t = 560 pA. (c) The STM image shows the coexistence of a **3N** close-packed structure and the **3N**/**3F3I** network. Tunneling conditions: V_{bias} = 770 mV, I_t = 438 pA. (d) High-resolution STM image of the **3N**/**3F3I** honeycomb structure. Tunneling conditions: V_{bias} = 888 mV, I_t = 1060 pA. (e) Structural model of the **3N**/**3F3I** honeycomb structure. Possible XBs are depicted by yellow dashed lines.

self-assembly structure of the XB donor **3F3I** and XB acceptor **3N**. The **3N** molecule has a strong adsorption affinity to HOPG and can absorb directly on octylbenzene (OB)/HOPG surface in a close-packed manner, in agreement with the literature[8] (Figure S1). No ordered adsorption structures of XB donor **3F3I** on the HOPG surface were observed.

The detailed experimental process for the fabrication of the binary XB molecular assembly is provided in the Supporting Information. In brief, the STM tip is preloaded with both XB donor and acceptor molecules. Then, it is used to scan a HOPG surface that has been freshly cleaved and covered with OB liquid film. After applying several electrical pulses at 3.6 V during the scanning process, a highly ordered **3N**/**3F3I** honeycomb network was obtained (Figure 1b). By comparing with the atomic image of the underlying HOPG lattice, the **3N**/**3F3I** honeycomb structure was determined to grow at 19° relative to the main symmetry axes of the underlying HOPG lattice (Figure S3). Figure 1c shows the coexistence of the monocomponent **3N** close-packed structure and the **3N**/**3F3I** network. The upper part of Figure 1c shows the **3N** close-packed structure, whereas the lower left part of the image shows the **3N**/**3F3I** network. The formation of the **3N**/**3F3I** honeycomb network can be routinely achieved by applying electrical pulses ranging from 3.4 to 4.2 V and a proper duration time (3 to 30 ms) of electric pulse (Figures S5 and S6). Figure 1d displays the high-resolution STM image of binary **3N**/**3F3I**. The lattice parameters outlined in Figure 1d were measured to be $a = b = 2.5 \pm 0.2$ nm, $\gamma = 60 \pm 2°$. The size of a typical honeycomb pore was in agreement with the expected size of 2.5 nm predicted by DFT calculations. Figure 1e shows the proposed structural model for the **3N**/**3F3I** honeycomb network. Each iodine atom (meta-position) per **3F3I** molecule forms XBs with its neighboring XB acceptor **3N** (as illustrated by the yellow dashed lines in Figure 1e). The distance of the N···I XB was ca. 2.5 Å, which is in good agreement with the lengths observed for the same interaction in organic crystals.[1d,3b]

We further chose ditopic **4F2I** as an XB donor to obtain an open porous network with larger pore diameters. As shown in Figure 2a, the **3N**/**4F2I** dyad is expected to form a honeycomb network structure only if XB is involved as an intermolecular interaction. This **3N**/**4F2I** honeycomb network would have a pore size of 4.8 nm based on DFT calculations (Figure S4). Under similar electrical pulse (3.6 to 4.2 V) experimental conditions, a more complex porous structure was obtained

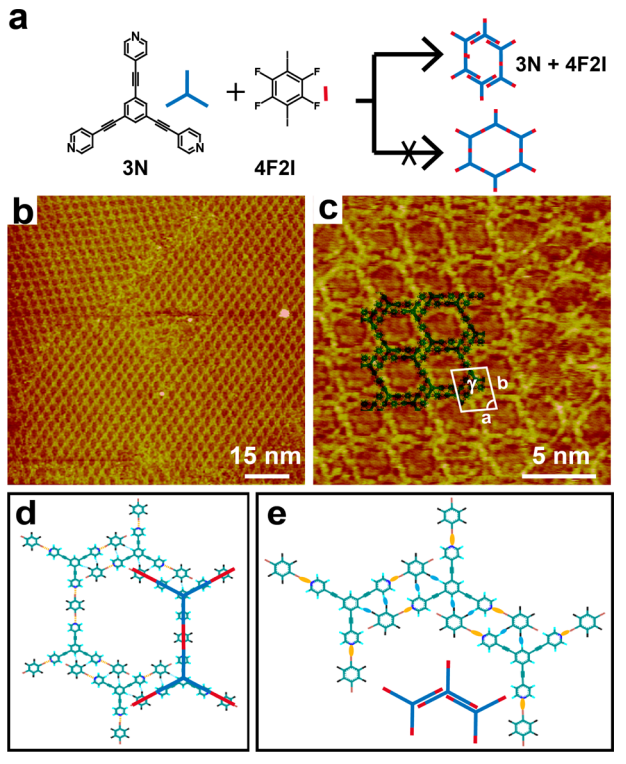

Figure 2. (a) Schematic diagram of the **3N**/**4F2I** self-assembled porous structure. (b) Large-scale STM image of the **3N**/**4F2I** porous structure. Tunneling conditions: V_{bias} = 679 mV, I_t = 450 pA. (c) High-resolution STM image of the **3N**/**4F2I** porous structure. Tunneling conditions: V_{bias} = 725 mV, I_t = 545 pA. (d) Structural model of the **3N**/**4F2I** porous structure. (e) Details of the **3N**/**4F2I** porous structure. The hydrogen bonds are schematically represented by blue spots. The XBs are schematically represented by yellow spots.

DOI: 10.1021/jacs.5b02206
J. Am. Chem. Soc. 2015, 137, 6128−6131

(Figure 2a, top). A large-scale STM image in Figure 2b shows the binary 2D porous supramolecular architecture. The bright areas correspond to the π-conjugated molecular regions due to their high electron densities, while the dark areas are voids in the network. The parameters of the unit cell outlined in Figure 2c are $a = 3.4 \pm 0.2$ nm, $b = 3.6 \pm 0.2$ nm, $\gamma = 79 \pm 2°$.The details of the molecular packing mode are revealed by high-resolution STM (Figure 2c). There are two branches antiparallel to each other in the *a* direction. Such an antiparallel arrangement can maximize overlap. Four C−H···F hydrogen bonds are formed as illustrated by the blue spots in Figure 2e. This antiparallel arrangement of the fluorinated rigid molecules was stabilized by −H···F hydrogen bonds, a well-documented motif.[9] The **3N**/**4F2I** porous structure was sustained by both hydrogen bonds (blue spots in Figure 2e) and XBs (yellow spots in Figure 2e) in *a* direction. There is only one chain lying in the *b* direction. There are two **3N** molecules connected to each with a head-to-head orientation. The distance between the two **3N** molecules was measured to be 2.7 nm, which is longer than the sun of two **3N** branches (0.7 nm). There is a **4F2I** node connecting two **3N** molecules. Two XBs are formed between the two iodine atoms and the pyridyl groups of the **3N** molecules, as illustrated by the model superimposed in Figure 2d.

Interestingly, we observed an anisotropic stability difference in the *a* and *b* directions of the **3N**/**4F2I** porous structure. The molecule arrays in the *b* direction were sensitive to STM tip scanning, while the molecule arrays in the *a* direction were stable (Figure S7). This phenomenon is presumably due to the stronger interactions along the *a* direction than the *b* direction. As shown in the structural model, the *a* direction is stabilized by multiple intermolecular interactions, and the *b* direction is stabilized by two XBs only. Thus, defects easily arise along the *b* direction.

Generally speaking, nanoporous monolayers are thermodynamically less stable than their densely packed structural counterparts due to the close-packing principle.[10] The absence of fully XB-sustained honeycomb structures (e.g., the structure in Figure 2a, bottom) with such open frameworks can be ascribed to the insufficient strength of XB to support a large open porous network.

To demonstrate the role of XB in the formation of porous structures, we carried out two control experiments (Scheme S1). First, we used **4H2I**, which is structurally similar to **4F2I** except that the F atoms are replaced by H atoms, to coassemble with **3N** molecules. Under the same experimental conditions, we did not observe any ordered adlayers except for some disordered domains (Figure S8). This experiment shows that the electron-withdrawing F atoms are important. Second, the perfluorobenzene (**6FB**), which has no iodine group to interact with the pyridyl group to form XB, failed to form any XB-based monolayers under similar conditions. Overall, we conclude that the porous structure of the **3N** and XB donor systems is primarily stabilized by XB interactions.

We found that the electrical manipulation method is a general method to engineer XB-based structures. By varying the XB acceptors across various pyridyl derivatives (ditopic, tetratopic), different XB-based binary supramolecular structures were obtained. In these cases, the simple ditopic **4F2I** was chosen as the XB donor. Molecules of **2N** and **4N** were each used as an XB acceptors. Figure 3a shows the formation of a **2N**/**4F2I** XB-based linear structure. Pure **2N** cannot be observed on HOPG surfaces due to the high mobility of the molecules. Figure 3a shows that the **2N** molecules interacted with **4F2I** via the two pyridyl groups to form a binary XB-based linear structure. The

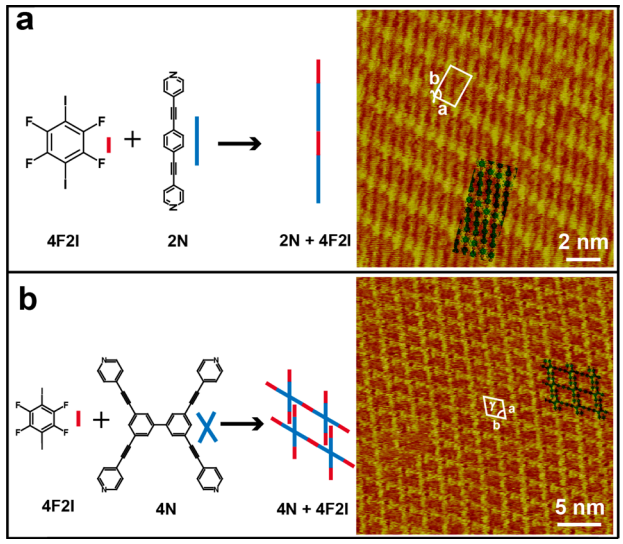

Figure 3. Formation of a series of binary XB-based supramolecular structures between the **4F2I** ditopic donor and other XB acceptors. (a) The formation of a **2N**/**4F2I** XB-based linear structure. High-resolution STM image of the **2N**/**4F2I** linear structure. Tunneling conditions: V_{bias} = 758 mV, I_t = 513 pA. (b) The formation of the **4N**/**4F2I** XB-based porous structure. High-resolution STM image of the **4N**/**4F2I** porous structure. Tunneling conditions: V_{bias} = 766 mV, I_t = 452 pA.

bright spots in the STM image are attributed to **4F2I** molecules. The dark rods are attributed to **2N** molecules. Details of the **2N**/**4F2I** linear structures are discussed in Figure S9. Figure 3b shows the formation of a **4N**/**4F2I** XB-based porous structure. The pure **4N** can form a close-packed structure on HOPG surfaces (Figure S2). The **4N**/**4F2I** binary system formed a tetragonal XB-based porous structure. Detailed structural analysis (Figure S10) indicates that the structure is stabilized by a combination of hydrogen bonding and XB, similar to what was observed for the **3N**/**4F2I** binary XB-based porous structure.

We found that the electrical manipulation was necessary for the formation of XB-based structures. The influence of the electrical pulse bias and the polarity on the structural outcome of the assembly was investigated. An XB-based structure (Figures S11 and S12) was formed only when the voltage of the applied electrical pulses ranged from 3.8 to 4.4 V. Changing the bias to negative did not furnish XB-based structures.

We should note that this tip modification method is only applied when **3N** is involved as the XB acceptor. If **3N**/**4F2I** or **3N**/**3F3I** were preloaded on the HOPG surface, only a monocomponent **3N** close-packed structure was observed, independent of the applied electrical pulses (Figure S13). The **3N** was preferentially adsorbed on the HOPG surface, and the electric stimulus was insufficient to change the close-packed adsorption behavior of **3N** once it adsorbed. Thus, we adopted a method to treat the STM tip with a solution of **3N**/**4F2I** to avoid the strong affinity of **3N** to HOPG. In contrast, the tip modifying method is not necessary for other XB-based structures utilizing **2N** and **4N** (Figures S11 and S12).

The binding energy of N−I XB is reported to be 5−30 kJmol^{-1} by theoretical calculations and experimental determinations.[1b,4a,5b] As **3N** and **3F3I** cannot form the expected open porous structure directly, we assume that the binding energy of XB is insufficient for the formation of an open network. One hypothesis for the electric stimuli-induced XB assembly is that the XB strength is transiently enhanced by electrical pulses. As

DOI: 10.1021/jacs.5b02206
J. Am. Chem. Soc. 2015, 137, 6128−6131

demonstrated by theoretical calculations, XB can be enhanced several fold when a positive charge is in close proximity to the halogen atom.[11,4e] Charge-assisted XB has been observed in several molecular systems in the solution phase.[4e,12] Under the experiential conditions presented in this work, the application of the electric stimuli may induce a transient change in the electrostatic distribution of the XB donor, which can then form stronger XB and sustain an XB-based open porous network. We note that there are many studies about electric stimuli induced change of electronic states of adsorbates on surfaces.[13] This hypothesis is consistent with the result that the process can only be induced by positive pulses and in a well-defined bias range. The control experiments indicate that XB donors do not change their chemical state after applying electric pulses (Figures S14 and S15, Table S1). Further understanding of the mechanism of electric stimuli induced XB interactions by theoretical calculations is currently under investigation.

In summary, we have found a new strategy to fabricate binary XB-based supramolecular structures. By applying electrical pulses during assembly, binary nanoporous networks with XB as the driving force were demonstrated. Although XB has been studied in crystal engineering, it is used here for the first time to fabricate binary XB-based open networks on surfaces. Furthermore, a series of XB-based porous structures have been successfully obtained using this approach. This design strategy has been shown to hold promise as a new strategy to fabricate XB-based materials.

■ ASSOCIATED CONTENT

Supporting Information

Additional experimental details, STM images, and data analysis. The Supporting Information is available free of charge on the ACS Publications website at DOI: 10.1021/jacs.5b02206.

■ AUTHOR INFORMATION

Corresponding Authors

*wangd@iccas.ac.cn

*wanlijun@iccas.ac.cn

Notes

The authors declare no competing financial interest.

■ ACKNOWLEDGMENTS

Special thanks go to Dr. F. Y. Wang and Dr. Q. Luo of ICCAS for SIMS data acquirement. This work is supported by National Key Project on Basic Research (Grants 2011CB808701 and 2011CB932304), National Natural Science Foundation of China (Grants 21127901, 21233010, 21373236), and Strategic Priority Research Program of the Chinese Academy of Sciences (Grant No. XDB12020100). P.J.S. thanks the NSF (CHE 0820955) for financial support.

■ REFERENCES

(1) (a) Metrangolo, P.; Meyer, F.; Pilati, T.; Resnati, G.; Terraneo, G. *Angew. Chem., Int. Ed.* **2008**, *47*, 6114. (b) Erdelyi, M. *Chem. Soc. Rev.* **2012**, *41*, 3547. (c) Friščić, T. *Chem. Soc. Rev.* **2012**, *41*, 3493. (d) Metrangolo, P.; Resnati, G. *Chem.—Eur. J.* **2001**, *7*, 2511. (e) Hassel, O.; Strømme, K. O. *Nature* **1958**, *182*, 1155. (f) Schmidt, G. M. J. *Pure Appl. Chem.* **1971**, *27*, 647. and references therein (g) Cohen, M. D.; Schmidt, G. M. J.; Sonntag, F. I. *J. Chem. Soc.* **1964**, 2000. (h) Schmidt, G. M. J. *J. Chem. Soc.* **1964**, 2014.

(2) (a) Ramasubbu, N.; Parthasarathy, R.; Murray-Rust, P. *J. Am. Chem. Soc.* **1986**, *108*, 4308. (b) Zordan, F.; Brammer, L.; Sherwood, P. *J. Am. Chem. Soc.* **2005**, *127*, 5979.

(3) (a) Lieffrig, J.; Jeannin, O.; Fourmigué, M. *J. Am. Chem. Soc.* **2013**, *135*, 6200. (b) Aakeröy, C. B.; Chopade, P. D.; Desper, J. *Cryst. Growth Des.* **2011**, *11*, 5333. (c) Ji, B.; Wang, W.; Deng, D.; Zhang, Y. *Cryst. Growth Des.* **2011**, *11*, 3622. (d) Pfrunder, M. C.; Micallef, A. S.; Rintoul, L.; Arnold, D. P.; Davy, K. J.; McMurtrie, J. *Cryst. Growth Des.* **2012**, *12*, 714.

(4) (a) Libri, S.; Jasim, N. A.; Perutz, R. N.; Brammer, L. *J. Am. Chem. Soc.* **2008**, *130*, 7842. (b) Fox, D. B.; Liantonio, R.; Metrangolo, P.; Pilati, T.; Resnati, G. *J. Fluor. Chem.* **2004**, *125*, 271. (c) Metrangolo, P.; Pilati, T.; Resnati, G.; Stevenazzi, A. *Curr. Opin. Colloid Interface Sci.* **2003**, *8*, 215. (d) Tsuzuki, S.; Wakisaka, A.; Ono, T.; Sonoda, T. *Chem.—Eur. J.* **2012**, *18*, 951. (e) Carlsson, A.-C. C.; Gräfenstein, J. r.; Budnjo, A.; Laurila, J. L.; Bergquist, J.; Karim, A.; Kleinmaier, R.; Brath, U.; Erdélyi, M. *J. Am. Chem. Soc.* **2012**, *134*, 5706.

(5) (a) Boterashvili, M.; Lahav, M.; Shankar, S.; Facchetti, A.; van der Boom, M. E. *J. Am. Chem. Soc.* **2014**, *136*, 11926. (b) Meazza, L.; Foster, J. A.; Fucke, K.; Metrangolo, P.; Resnati, G.; Steed, J. W. *Nat. Chem.* **2012**, *5*, 42. (c) Priimagi, A.; Saccone, M.; Cavallo, G.; Shishido, A.; Pilati, T.; Metrangolo, P.; Resnati, G. *Adv. Mater.* **2012**, *24*, 345. (d) Bolton, O.; Lee, K.; Kim, H.-J.; Lin, K. Y.; Kim, J. *Nat. Chem.* **2011**, *3*, 205. (e) Shirman, T.; Freeman, D.; Posner, Y. D.; Feldman, I.; Facchetti, A.; van der Boom, M. E. *J. Am. Chem. Soc.* **2008**, *130*, 8162.

(6) Priimagi, A.; Cavallo, G.; Metrangolo, P.; Resnati, G. *Acc. Chem. Res.* **2013**, *46*, 2686.

(7) (a) Gutzler, R.; Ivasenko, O.; Fu, C.; Brusso, J. L.; Rosei, F.; Perepichka, D. F. *Chem. Commun.* **2011**, *47*, 9453. (b) Gutzler, R.; Fu, C.; Dadvand, A.; Hua, Y.; MacLeod, J. M.; Rosei, F.; Perepichka, D. F. *Nanoscale* **2012**, *4*, 5965. (c) Yoon, J. K.; Son, W.-j.; Chung, K.-H.; Kim, H.; Han, S.; Kahng, S.-J. *J. Phys. Chem. C* **2011**, *115*, 2297. (d) Silly, F. *J. Phys. Chem. C* **2013**, *117*, 20244. (e) Gatti, R.; MacLeod, J. M.; Lipton-Duffin, J. A.; Moiseev, A. G.; Perepichka, D. F.; Rosei, F. *J. Phys. Chem. C* **2014**, *118*, 25505.

(8) Ciesielski, A.; Szabelski, P. J.; Rżysko, W.; Cadeddu, A.; Cook, T. R.; Stang, P. J.; Samorì, P. *J. Am. Chem. Soc.* **2013**, *135*, 6942.

(9) Mu, Z.; Shu, L.; Fuchs, H.; Mayor, M.; Chi, L. *J. Am. Chem. Soc.* **2008**, *130*, 10840.

(10) (a) Desiraju, G. R. *Angew. Chem., Int. Ed.* **2007**, *46*, 8342. (b) Desiraju, G. R. *Angew. Chem., Int. Ed.* **1995**, *34*, 2311.

(11) (a) Zou, J. W.; Jiang, Y. J.; Guo, M.; Hu, G. X.; Zhang, B.; Liu, H. C.; Yu, Q. S. *Chem.—Eur. J.* **2005**, *11*, 740. (b) Serpell, C. J.; Kilah, N. L.; Costa, P. J.; Félix, V.; Beer, P. D. *Angew. Chem., Int. Ed.* **2010**, *49*, 5322.

(12) Kilah, N. L.; Wise, M. D.; Serpell, C. J.; Thompson, A. L.; White, N. G.; Christensen, K. E.; Beer, P. D. *J. Am. Chem. Soc.* **2010**, *132*, 11893.

(13) (a) Alemani, M.; Peters, M. V.; Hecht, S.; Rieder, K.-H.; Moresco, F.; Grill, L. *J. Am. Chem. Soc.* **2006**, *128*, 14446. (b) Jiang, Y.; Huan, Q.; Fabris, L.; Bazan, G. C.; Ho, W. *Nat. Chem.* **2013**, *5*, 36.

DOI: 10.1021/jacs.5b02206
J. Am. Chem. Soc. 2015, 137, 6128−6131